ADVANCED MATERIALS INTERFACES
www.advmatinterfaces.de

Tapered Cross Section Photoelectron Spectroscopy Provides Insights into the Buried Interfaces of III-V Semiconductor Devices

Clément Maheu, Mohammad Amin Zare Pour, Iban Damestoy, David Ostheimer, Maximilian Mellin, Dominik C. Moritz, Agnieszka Paszuk, Wolfram Jaegermann, Thomas Mayer, Thomas Hannappel, and Jan P. Hofmann**

Interfaces are key elements that define electronic properties of the final device. Inevitably, most of the active interfaces of III–V semiconductor devices are buried and it is therefore not straightforward to characterize them. The Tapered Cross Section Photoelectron Spectroscopy (TCS-PES) approach is promising to address such a challenge. That the TCS-PES can be used to study the relevant heterojunction in epitaxial III–V architectures prepared by metalorganic chemical vapor deposition is demonstrated here. A MULTIPREP polishing system that enables controlling the angle between the sample holder and the polishing plate has been employed to improve the reproducibility of the polishing procedure. With this procedure, that preparing the TCS of III–V semiconductor devices with tapering angles lower than 0.02° is possible is demonstrated. The PES provides then information about the buried interfaces of Ge|GaInP and GaAs|GaInP layer stacks. Both, chemical and electronic properties have been measured by PES. It evidences that the preparation of the TCSs under an uncontrolled atmosphere modifies the pristine properties of the critical buried heterointerfaces. Surface states and reaction layers are created on the TCS surface, which restrict unambiguous conclusions on buried interface energetics.

1. Introduction

The optoelectronic properties of multinary III–V semiconductors, their tunable band gap, reliable control of doping concentrations and the formation of functional heterostructures such as tunnel junctions make them promising candidates for various high-performance device applications, for example, tandem photovoltaic devices[1–3] or photoelectrodes.[4–6] Commonly, Ge(100) or GaAs(100) substrates, gallium indium phosphide (GaInP), and gallium arsenide (GaAs) buffer layers play key roles in these architectures.

GaInP, for example, has an ideal bandgap engineering potential and is commonly grown as a top photoabsorber in record photovoltaic layer structures[1] with either lattice-matched stoichiometry ($Ga_{0.51}In_{0.49}P$) to GaAs(100) on Ge(100) substrates,[7] or to an underlying GaInAs bottom solar cell.[2]

But even more than the intrinsic properties of the individual layers, their interfaces might govern the overall properties of the device.[8,9] Therefore, investigating the properties of such buried interfaces, such as band alignment and space charge layers induced by defect formation or chemical modifications, is crucial for addressing the efficiency losses of these devices. However, inevitably, the buried interfaces inside III–V semiconductor devices are not straightforward to characterize with modern surface science methods.[10] As a first-of-its-kind study of the relevant AlInP|GaInP (100) interface[11,12] we present here an experimental investigation by Tapered Cross Section (TCS) Photoelectron Spectroscopy (PES) (TCS-PES) of GaInP(100) grown on Ge(100) and GaAs(100) substrates.

PES is one of the few techniques that provides spectroscopic chemical and electronic information at the same time. However, PES is a surface sensitive method with an information depth in the nanometer range. 95% of the photoelectrons emitted from interfaces buried by an upper layer thicker than 3 times the inelastic mean free path (IMFP – λ) of the photoelectrons will be blocked, which impedes the analysis of the buried interface. A standard procedure to access these buried interfaces is to cut a sample by focused ion-beam (FIB) creating

C. Maheu, I. Damestoy, M. Mellin, D. C. Moritz, W. Jaegermann, T. Mayer, J. P. Hofmann
Surface Science Laboratory
Department of Materials and Earth Sciences
Technical University of Darmstadt
Otto-Berndt-Strasse 3 64287, Darmstadt, Germany
E-mail: cmaheu@surface.tu-darmstadt.de; hofmann@surface.tu-darmstadt.de

M. A. Zare Pour, D. Ostheimer, A. Paszuk, T. Hannappel
Fundamentals of Energy Materials
Institute of Physics
Ilmenau University of Technology
Gustav-Kirchhoff-Strasse 5 98693, Ilmenau, Germany

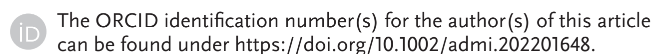
The ORCID identification number(s) for the author(s) of this article can be found under https://doi.org/10.1002/admi.202201648.

© 2022 The Authors. Advanced Materials Interfaces published by Wiley-VCH GmbH. This is an open access article under the terms of the Creative Commons Attribution License, which permits use, distribution and reproduction in any medium, provided the original work is properly cited.

DOI: 10.1002/admi.202201648

a normal cross section with a size that is usually below 1 µm. It is thus one or two orders of magnitude smaller than the lateral resolution of a lab-based PES setup and buried interfaces cannot be directly assessed by PES. Other characterization techniques with the required nanometer-resolution have been used, though. Among them, electron microscopies are valuable tools for acquiring defect densities and the structure of the involved interfaces down to the atomic level. For instance, they reveal the interfaces between GaP and Si as well as the interfaces between the bulk GaP and the numerous antiphase domains.[13,14] Four-dimensional scanning transmission electron microscopy (4D-STEM) has recently characterized GaAs-based p–n junctions.[15] The GaAs|GaInP interface has also been studied extensively by scanning tunneling microscopy and spectroscopy,[16] scanning transmission electron microscopy,[17] as well as photoluminescence and Hall measurements.[18] All these studies concluded with the formation of extra multinary interlayers (GaInAs, GaAsP, or even GaInAsP). However, these techniques provide either electronic or chemical information while PES in principle may provide both at the same time. Depth-profiling XPS confirmed the tendency of In to segregate at the GaAs|GaInP interface and give rise to mixed phases.[19,20]

Strategies to investigate buried interfaces with PES can be divided into two main groups: bottom–up and top–down approaches. The first strategy mainly consists of so-called interface experiments. Those consist of alternating between the stepwise deposition of a thin layer of a contact material on top of a substrate material and the measurement of the resulting deposit and formed junctions by PES to provide spectroscopic information on the emerging contact. Examples of junctions formed with different materials may be found in these works.[10,21] That way, one interface can be studied at a time. It also requires an integrated ultra-high vacuum cluster tool system to avoid contamination between the deposition and the measurement steps. It also means that only vacuum deposited samples can be studied, while most of the time their properties differ from those of their counterparts prepared in the original deposition apparatus.

The top–down approach, on the other hand, starts directly with a full device stack. It includes PES depth-profiling methods for which ion gun etching cycles and PES measurements are alternated.[19,20,22] In these works, Romanyuk et al. combined XPS with Ar gas cluster ion beam sputtering, they studied the GaP/Si(001) interface and the addition of As to suppress the formation of antiphase domains.[20,22] The top–down approach also includes the more recent TCS-PES method. A TCS is a very low-angle cross section that is extended enough so that nanometer-sized structures can be resolved despite the tens of micrometers lateral resolution of the PES. Indeed, creating an angle lower than 0.1° between the horizontal part of the device and the resulting cross section converts a normal cross section of hundred nanometers into a TCS of a few millimeters. Having such a TCS provides areas that can be analyzed by PES as individual layers or as an interface between two layers. If no modifications are induced during the TCS preparation by, for instance, the polishing procedure, then, the TCS-PES approach provides the chemical composition of the layers and potential variation of space charge regions at the interface of the full device.

Until now proof of concepts have been reported on perovskite solar cells[23–25] but, to the best of our knowledge, it is the first time that TCS-PES is performed on III–V semiconductor devices. In addition, until now, TCSs were prepared by manual polishing procedures[23,24] or using a drilling machine,[25] leading to issues with reproducibility of the prepared cross sections.

We present here the first attempt using a MULTIPREP polishing system that enables to control the angle between the sample holder and the polishing plate with an accuracy of 0.02°. TCS-PES experiments were performed on two III–V semiconductor devices prepared by metalorganic chemical vapor deposition (MOCVD): Ge|GaInP and GaAs|GaInP.

2. Results and Discussion

2.1. Tapered Cross Section Preparation and Characterization

The TCS-PES was until now only applied to hybrid perovskite solar cells. Here, we aim to extend the scope of TCS-PES to III–V semiconductor devices. In contrast to soft materials like organic–inorganic perovskites, organic hole extraction layers and gold contacts that compose perovskite solar cells, III–V materials are much stiffer and brittle. For that reason, we used a mechanical polishing machine where the force applied to the sample can be adjusted (see Figure S1, Supporting Information). The machine also allows applying radial and axial angles to create the targeted TCS. An increment of 0.02° can be used for the adjustment of the angle. The MULTIPREP polishing system seems to provide a more controlled way to prepare the TCS than manual polishing techniques although more TCS samples would be required to confirm such a statement. Controlling the tapering angle is crucial as it defines the length of the tapered part (i.e., the tapered width) that directly relates to the magnification of the normal cross section when projected to the TCS. The smaller the tapering angle is, the larger the tapered width is, and the easier it is to distinguish the different layers of the sample and the details of their interfaces. Thanks to this low angle, nanometer-sized structures on the normal cross section are projected onto the millimeter-sized TCS. It should also be mentioned that gluing the sample to the sample holder is a critical step because it can induce small angles unintentionally. It explains why some of the TCSs were obtained without applying any angle (see Table S1, Supporting Information).

We chose to polish the sample without using any liquid, which allowed for better control of the angle between the polishing plate and the sample, minimized the chance of chemical modification due to remnants and possible reaction products but also increased the chance of cross contamination and of reaching locally high temperatures that can alter the composition of the sample by for instance air oxidation. For minimizing contamination, the sample is polished on the same area of the polishing paper for a limited time. For minimizing overheating, a relatively low rotation speed of the polishing plate has been used. No oscillation was applied to not alter the targeted geometry. Indeed, oscillation would have varied the angle between the normal axis of the sample and the tangent of the polishing paper. It can, however, be observed by eye that some of the removed materials accumulate on the sample and might alter the results of the XPS line scan measurements (see Figure S1b, Supporting Information).

© 2022 The Authors. Advanced Materials Interfaces published by Wiley-VCH GmbH

In comparison to the undistinguishable (by eye at least) layers composing the perovskite solar cells, the III–V layers are shiny, it is feasible to distinguish the GaAs substrate and the GaInP layer (see Figure S1b, Supporting Information). In this image, the white stripes indicated by the red arrows seem to be an oxide layer on the TCS between the Ge and the GaInP. This oxide layer is also observed by scanning electron microscopy (SEM) (see Figure S2, Supporting Information) and its thickness is estimated to be 15–20 µm. Another hypothesis on the origin of these white stripes is the breaking of the thin GaInP layer and the resulting rough surface reflects the light in a way that it appears white. A direct proof of the success of the TCS preparation is highly valued for refining polishing parameters on a sample. With an optical microscope, it can also be seen that the geometry of the sample is no longer a parallelepiped (see Figure S1c, Supporting Information), a significant amount of material was removed toward the right of the sample giving access to the buried GaAs|GaInP interface.

Such a TCS interface can also be characterized using SEM (see **Figure 1**b). From each side of the interface on the TCS, energy dispersive X-ray (EDX) measurements have been performed and reveal a stoichiometry close to 1:1 for the GaAs and close to 1.2:1 (Ga:P) and 0.5:1 (In:P) for the top layer (see Figure 1c). A non-negligible amount of carbon was also detected at the surface of the sample. This is mostly due to the polishing procedure in air and the use of diamond lapping films. Additional SEM pictures and EDX mapping of the Ge|GaInP and GaAs|GaInP interfaces are provided in Figures S2 and S3, Supporting Information.

Therefore, we demonstrate here that it is feasible to prepare TCSs of III–V semiconductor devices with the MULTIPREP polishing system.

2.2. Insights into Buried Interfaces by TCS-PES and Limitations

The TCSs of Ge|GaInP and GaAs|GaInP were then characterized by performing XPS line scans. The samples are discussed in order of increasing complexity.

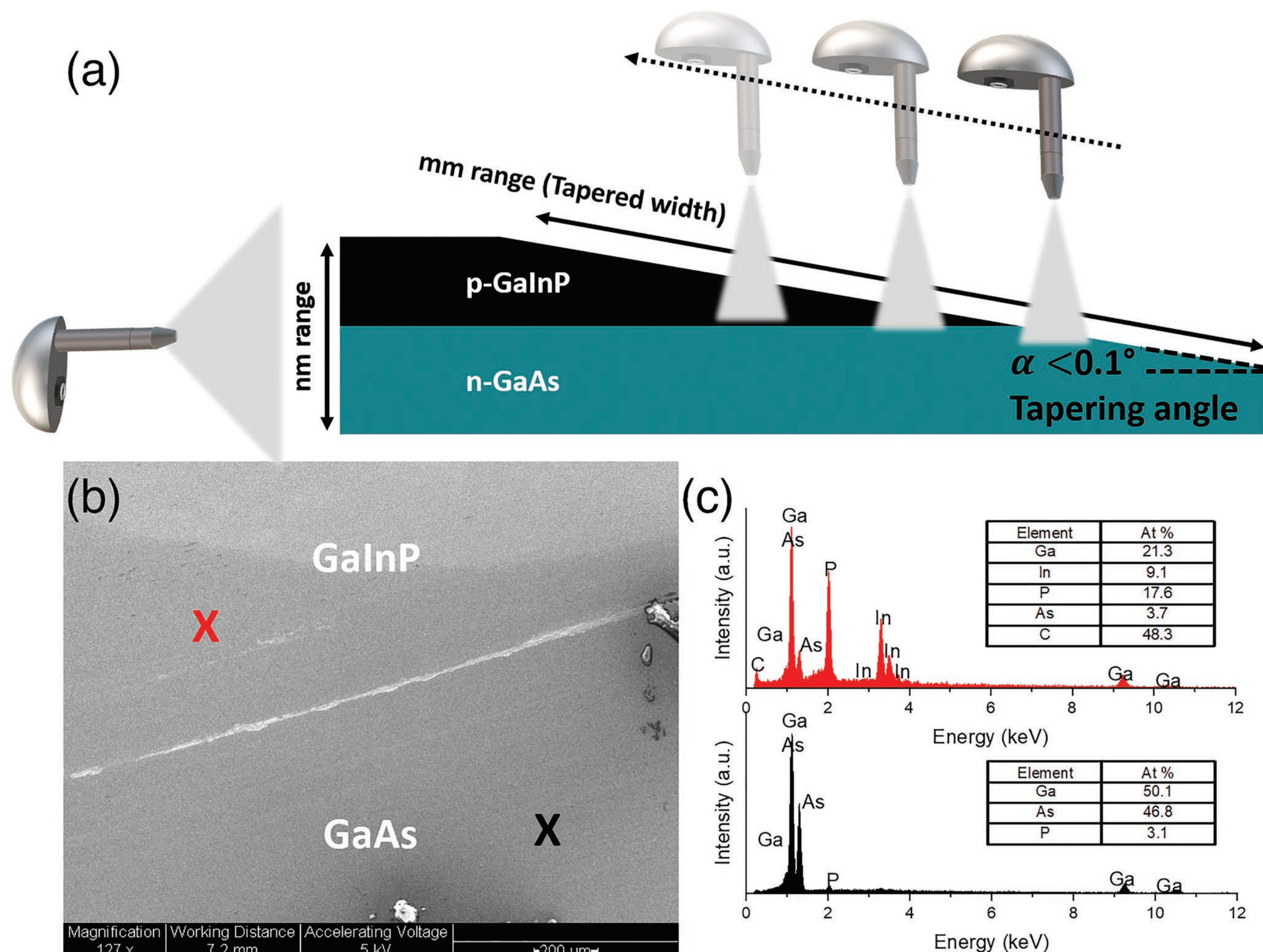

Figure 1. The top scheme (a) explains the Tapered Cross Section PES approach showing the projection of nanometer-sized structures on the normal cross section into millimeter-sized structures on the shallow angle tapered cross section. On the normal cross section on the left, the electron energy analyzer acceptance angle prevents local resolution of details of the interface while on the tapered cross section the details can be locally resolved. Scheme (a) is not drawn to scale. The bottom images depict the GaAs|GaInP interface as observed by SEM (b) and corresponding EDX measurements (c) of either side of the interface as indicated by the red (GaInP) and black (GaAs) crosses.

© 2022 The Authors. Advanced Materials Interfaces published by Wiley-VCH GmbH

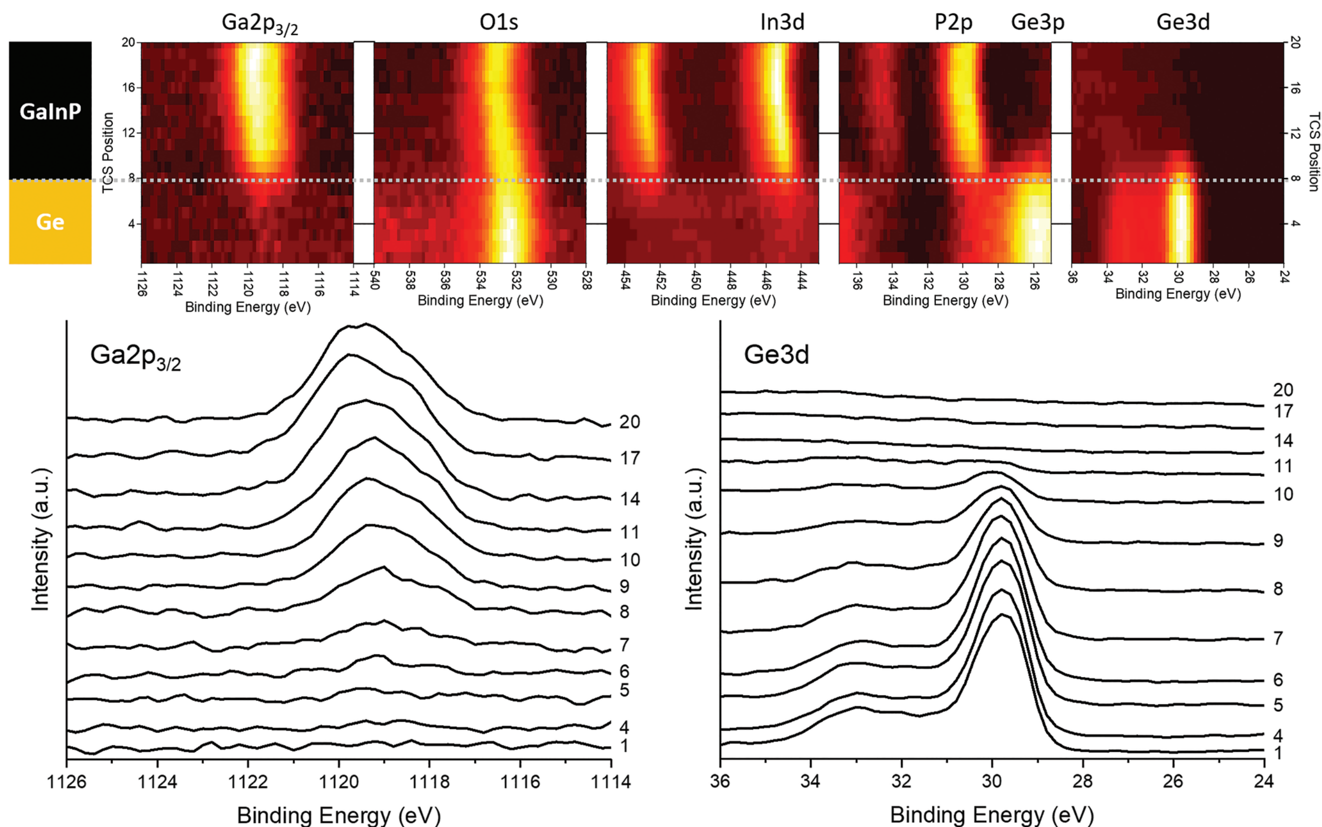

Figure 2. (Top) intensity contour maps of the tapered cross section XPS line scans of the core levels of Ga, O, In, P, and Ge. Core level spectra were recorded at different positions with a step width of 75 µm. The color code depicts the intensity of the XPS spectra. The element distribution indicates the interface position (white dots) between the two layers on the tapered cross section sketched on the left. (Bottom) corresponding $Ga2p_{3/2}$ and Ge3d core level spectra.

2.2.1. Case Study of p-Ge|p-GaInP

The first studied interface is the simplest one because it contains distinguishable elements: Ge on one side and Ga, In, and P on the other side. The core level spectra of the stepwise XPS line scans are depicted in **Figure 2** as intensity contour maps. On each position, from 1 to 20 XPS core level spectra of Ga2p, O1s, In3d, P2p, Ge3p and Ge3d were acquired. A color code is used, from dark to light colors, to show the intensity of each spectrum. White corresponds to the most intense peak of the series.

These intensity contour maps were used to identify the interface between Ge and GaInP. From the 1st to the 12th position, Ge has been detected while Ga, In and P are detected between the 6th and the 20th position. The difference in chemical composition between the two layers provides a clear demarcation: the 1st to the 5th positions correspond to pure Ge while the 13th to the 20th positions correspond to pure GaInP. Between the 6th and the 12th positions, contributions from both layers are detected. This can be due to fringes as well as intermixing of the layers but also to the depth of analysis of the XPS. Photoelectrons will be detected from up to a thickness equal to three times their inelastic mean free path (3λ). According to Equation (1),[26] the IMFPs of Ga2p and Ge3d core levels are estimated to be, respectively, 1.0 and 2.1 nm:

$$\lambda(E_{\text{kin}}) = \frac{143}{(E_{\text{kin}})^2} + 0.054 \times \sqrt{E_{\text{kin}}} \tag{1}$$

Therefore, the electrons from the Ge3d ($E_{\text{kin}} \approx 1457$ eV) will be still detected under the GaInP up to a GaInP thickness of 6.3 nm ($3 \times \lambda_{\text{Ge3d}}$).

Looking at the $Ga2p_{3/2}$ and Ge3d core level intensities in Figure 2 as well as the P2p and Ge3d spectra, we estimate the interface at position 8.

There is a 900 µm distance between the last point measurement on the TCS (position 20) and the interface (position 8). This means, based on a nominal thickness of 200 nm for the GaInP layer, that the TCS angle is at most 0.013°. Detailed calculations are provided in Figure S4, Supporting Information. However, it is unclear if position 20 still corresponds to the TCS or if it is measured on an unpolished part of the sample. Another way to estimate the TCS angle is to consider that from positions 10 to 11 the Ge3d state is not detected anymore. So, there is at least a GaInP thickness of 6.3 nm, according to the discussion above, between the measured point (position 11) and the buried interface. For this sample, the step width was 75 µm between each position. On the TCS, the interface is at position 8, that is, 225 µm away from position 11. This corresponds to a tapering angle of 0.002°. In both cases, it is evidenced that the TCS angle is low, even lower than the 0.02° accuracy that

© 2022 The Authors. Advanced Materials Interfaces published by Wiley-VCH GmbH

the MULTIPREP can provide, and it might explain why reproducing such an angle is challenging from an experimental point of view.

Such a low angle explains why we succeed to prepare the TCS even if the angle between the sample holder and the polishing plate of the MULTIPREP polishing system was set to zero. Despite all the precautions taken, the needed precision for a defined TCS angle is beyond what can be reached with the used polishing setup. We presume that, for example, the glue layer between sample and sample holder has a non-constant thickness. Perfect control of the TCS is however not mandatory to expose the buried interface of this junction. It is nonetheless important to be aware of it because it might induce slight deviations in the reproducibility of the TCS preparation.

Total emission intensities of Ga, In, P, Ge, and O core levels were integrated (i.e., without distinction between the different states) to obtain their relative concentrations along the TCS that are depicted in **Figure 3**. The drop of the Ge elemental concentration and the rise of Ga, In, and P ones confirm an interface centered at the 8th position. In3d emission is already evidenced at position 5, Ga at position 6, and P at position 9. This might indicate a tendency of In segregation, which was observed at a GaAs|GaInP interface,[19] or interdiffusion into the Ge layer. It can also be noticed that the P, In, and Ga stoichiometries do not fulfill the expected $Ga_{0.5}In_{0.5}P$ composition but indicate an over stoichiometry of In, 0.6:1 (Ga:P) and 1.3:1 (In:P). This is in contradiction to the EDX measurements, but EDX is much less surface sensitive than XPS. The unexpected stoichiometry is most probably due to the presence of oxidized species that have been created during the polishing procedure. Indeed, O1s emissions are observed all along the TCS (see Figure 3) as well as additional Ga-, In-, Ge-, and P-based states at higher BE (see Figure 2). For the Ge substrate, the Ge^0 state doublet is measured at 29.5 and 30.1 eV; the state at 3.2 eV higher BE corresponds to Ge^{IV} (GeO_2), and the one at 0.9 eV higher BE corresponds to an intermediate GeO_x state (see Figure S5, Supporting Information).[27,28] We quantified that almost half of the p-Ge(100) emission is related to oxidic species that presumably have formed during the polishing procedure. For instance, at position 1, the composition of the Ge states was the following: 48 at% for Ge^0, 25 at% for GeO_x, and 27 at% for GeO_2 (see Figure S5, Supporting Information, for the detailed fitting procedure of Ge3d). Similar findings were obtained for the GaInP layer: two states were identified for each of the Ga2p, In3d, and P2p core levels at 1118.5 and 1119.8 eV, at 445.2 and 445.8 eV, as well as at 129.8 and 134.4 eV, respectively. The absolute BE values vary from previous reports but the BE difference of 4.5 eV between the two P2p chemical states is the same and it is characteristic of the GaInP and the formation of $InPO_4$ or $In(PO_3)_3$.[4,29]

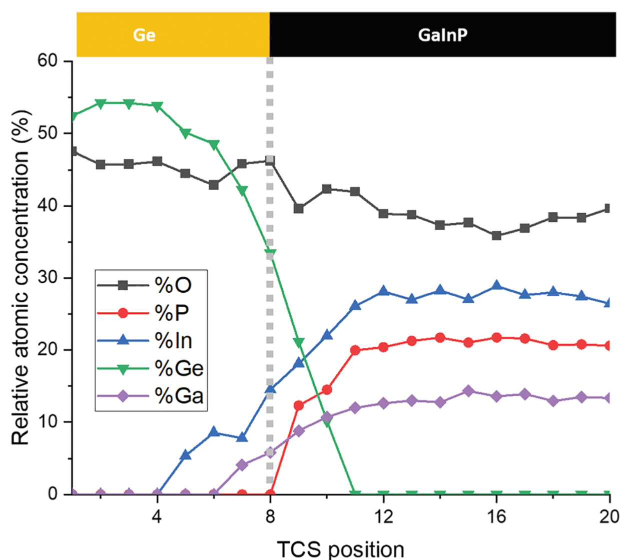

Figure 3. Relative atomic surface concentration of different elements (O, P, In, Ge, Ga) present across the tapered cross section Ge|GaInP. These concentrations were determined from the individual core level spectra across the tapered cross section. The full spectra were integrated without distinction between the different states. Core level spectra were recorded at different positions with a step of 75 µm.

A similar polishing procedure was performed on a second Ge|GaInP sample to obtain a second TCS and check the reproducibility of the oxide layer formation. The results are depicted in Figure S6, Supporting Information, and evidence the presence of GaO_x and $InPO_x$. This time, the two states for the Ga2p emissions lines are defined. Their quantification even shows that the amount of oxide increases at the expense of GaInP when moving closer to the interface. Polishing under ambient atmosphere is responsible for the emergence of these oxidized states. As the samples were polished dry, locally, the temperature may have also increased and accelerated the formation of these oxide layers. The stress that occurs during the polishing procedure might have been compensated through a reaction with ambient O_2 and H_2O.

If the polishing procedure induces significant deviation in the chemical composition of the interfaces, it limits the insights that can be provided by the TCS-PES methodology to the understanding of the III–V semiconductor devices. Such modifications were not observed or at least not pointed out when the TCS-PES was performed on perovskite solar cells. It appears that each class of material requires its specific strategy for the TCS preparation. Comparison with XPS depth profiling measurements or performing interface experiments would help to guide the development of a suitable TCS-PES strategy.

In Figure 2, it becomes clear from the intensity contour maps that at least the Ga2p, In3d, and P2p core levels were shifted to lower BE when moving from position 1 to the Ge|GaInP interface. To have a closer look at the BE shifts, first, the $Ga2p_{3/2}$, $In3d_{5/2}$, P2p and Ge3d core level spectra were fitted to discriminate the BE of the GaInP and Ge^0 states from the more oxidized ones. Then, the maxima of the GaInP and Ge^0 states were deduced (see Figures S5 and S7, Supporting Information). Finally, the BE shifts were calculated using reference BE measured for pure Ge (position 1–29.5 eV) and pure GaInP (position 20–129.7, 445.3, and 1118.4 eV). The result is shown in **Figure 4**. When moving closer to the interface, a shift to lower BE for the Ge3d core level, and a shift to higher BE for the elements composing the n-GaInP are observed.

Although in the perovskite case the binding energy shifts toward the interfaces could successfully be interpreted as the formation of space charge regions,[23] we doubt that this is the case on the III–V samples measured here. On a p-Ge to p-GaInP

© 2022 The Authors. Advanced Materials Interfaces published by Wiley-VCH GmbH

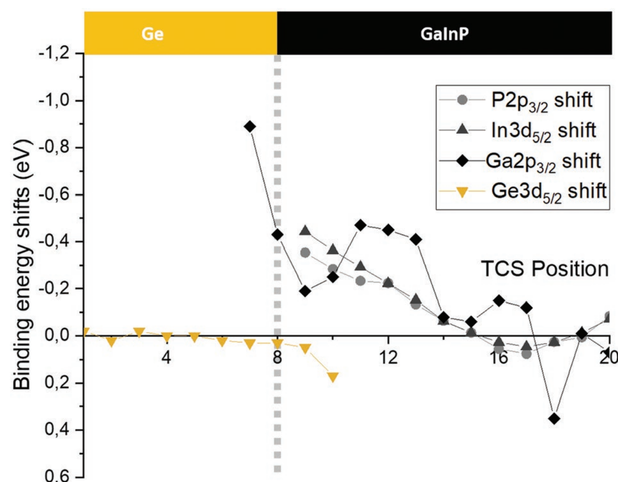

Figure 4. Binding energy shifts of $Ga2p_{3/2}$, $Ge3d_{5/2}$, $In3d_{5/2}$, and $P2p_{3/2}$ core level. The peak maxima of the Ge^0 and GaInP states are depicted in Figure S7, Supporting Information.

junction, no band bending is expected, and the III–V materials have a strong tendency to form gap states at the surface and at the interface with their oxides to which the TCS surfaces will be pinned. Therefore, we suppose, that the concentration of these gap states gradually varies along the TCS toward the interface, which leads to gradually varying pinning positions. The gradual increase of the oxidation of GaInP toward the TCS interface was indicated in the O2p intensity increase depicted in Figures 2 and 3, and Figure S5, Supporting Information.

These gap states lead to Fermi level pinning toward the exposed surface that alters the interface energetics across the junction. The energy difference between the valence band maximum (E_{VB}) and the Fermi level (E_F) was estimated (see Figure S8, Supporting Information). For position 1 (only Ge layer) and position 20 (only GaInP layer), $E_{VB} - E_F$ equal 0.4 and 1.2 eV, respectively. With E_g(Ge) = 0.67 eV, it means intrinsic or slightly n-type, and with E_g(GaInP) = 1.8 eV, it means an undeniable n-type.[8] This is in contradiction to the expected p-type behavior prepared during the synthesis. The energy resolution of the valence band spectra of Figures S7 and S12, Supporting Information, is however limited due to the low photoionization cross section of valence band states with Al K_α radiation when measuring the VB region with XPS.

Thus, the current state of the TCS prepared for the Ge|GaInP interface cannot reliably inform on the electronic properties of such an interface. Measures to form the TCS under controlled atmosphere or to remove the surface layers and/or passivate the surface states on the TCS will be developed in future TCS preparation protocols for III–V devices.

2.2.2. Case Study of n-GaAs|n-GaInP

The second interface, n-GaAs|n-GaInP, is more complex because it contains Ga in both layers. Only In and P on the one hand and As on the other hand allow us to distinguish the interface by elemental contrast. The results of the XPS line scans are depicted in **Figure 5** as intensity contour maps.

From the 1st to the 13th position, As has been detected while In and P are detected between the 9th and the 20th position. This can also be seen in Figure S9, Supporting Information, where the relative concentration profile of this interface is plotted. We, therefore, describe the TCS structure as follows: the 1st to the 8th positions correspond to the n-GaAs(100) wafer while the 14th to the 20th positions correspond to pure GaInP. Between these positions, there is the interface centered at position 10 (see white dotted line in Figure 5). The core level spectra of As3p and P2p (Figure 5) show the GaAs state, for which the intensity is declining, as well as the GaInP state, for which the intensity is rising. This can also be observed with the relative concentration profile depicted in Figure S9, Supporting Information.

With an interface centered at position 10, there is a 1500 µm distance between the top of the TCS (position 20) and the interface. Assuming a homogeneous polishing procedure, it means that the TCS angle is at best 0.015° or even below, if we use an alternative methodology as described in Figure S4, Supporting Information. This time, three polishing steps were used with an angle between the sample holder and the polishing plate of 0.1°, 0.06°, and 0.06°. Up to now, there is no unique polishing procedure that can be applied to all sample architectures. For each device, a polishing methodology needs to be developed. For the measurements of the perovskite solar cells, it was important to prepare the TCS by limiting water exposure, but for the III–V semiconductors it seems that the main issue is the polishing induced defects.

As before, the TCS-PES can lead to a relative concentration profile that helped to set the limit between the two materials and position the interface (see Figure S9, Supporting Information). BE shifts were also monitored over the TCS (see Figure S12, Supporting Information). When moving closer to the interface, a shift to higher BE for the elements composing the n-GaAs, and a shift to lower BE for the ones composing the n-GaInP are observed. These shifts can either come from Fermi level alignment or from chemical modifications induced by surface states.

For GaInP, oxidation states similar to those previously observed in the case of the Ge|GaInP interface were observed (see Figure S10, Supporting Information). This is valid for each of the Ga2p, In3d and P2p core levels with, for instance, the characteristic energy difference of 4.6 eV between the two P states indicating the formation of $InPO_4$ or $In(PO_3)_3$ (see Figure S10, Supporting Information).[4,29] On position 20 (pure GaInP) states with a BE of 1118.4 and 1119.9 eV were measured for the emission from the GaInP and the GaO_x, while on position 1 (pure GaAs), an asymmetric peak is visible and indicates GaAs at 1118 eV and a more oxidized compound at 1118.9 eV. This finding is in agreement with the two states observed for the As3d core level spectra, one centered at 41.4 eV and the other one centered at 3.1 eV higher in BE. The BE of the first state agrees with previous reports,[30–32] and the energy difference between the Ga2p and the As3d core levels is 1076.6 eV as in a previous work.[30] The relative energy difference of 3.1 eV between the two As3d core level states concludes the formation of As_2O_3 rather than As_2O_5.[33]

Valence band spectra were also recorded along the TCS (see Figure S13, Supporting Information). The energy differences of

© 2022 The Authors. Advanced Materials Interfaces published by Wiley-VCH GmbH

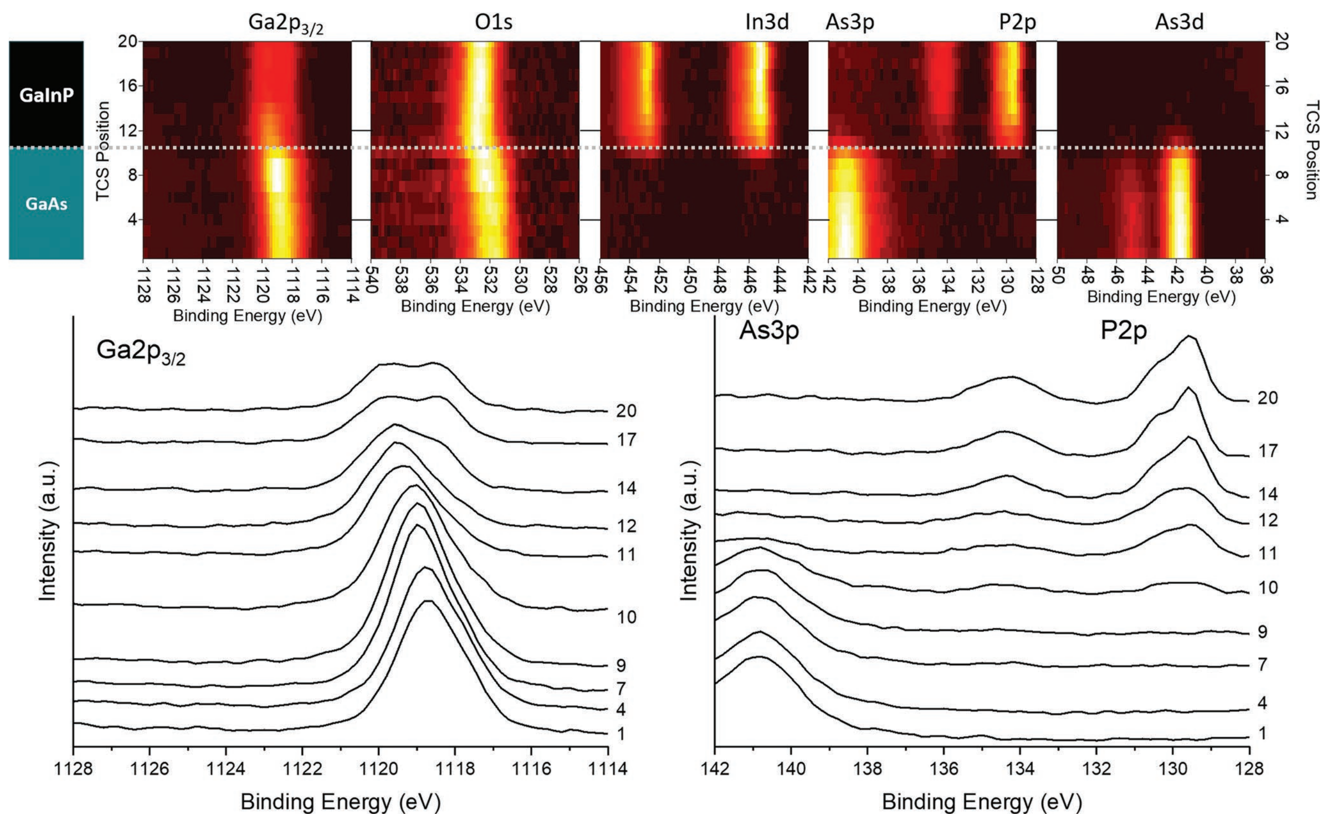

Figure 5. Intensity contour maps of the tapered cross section XPS line scans of the core levels of As, P, In, O, and Ga. Core level spectra were recorded at different positions with a step width of 150 µm. The color code depicts the intensity of the XPS spectra. The element distribution indicates the interface position (white dotted line) between the two layers on the tapered cross section sketched on the left. (Bottom) $Ga2p_{3/2}$, As3p and P2p core level spectra.

$E_F - E_{VB}$ for the pure compounds GaAs and GaInP equal 1.4 and 0.4 eV, respectively. GaAs has a band gap of 1.4 eV and the one of GaInP equals 1.8 eV.[8] It leads to a strongly n-type surface layer for the GaAs but, the $E_F - E_{VB}$ difference of GaInP is in contradiction with the synthesized bulk that should be n-type. For the two III–V semiconductor devices that have been studied, the Fermi level position of the GaInP was modified. On the p-Ge substrate, the GaInP was synthesized p-doped but, after the TCS preparation, the Fermi level on the TCS surface appears to be shifted to the conduction band. On the n-GaAs substrate, the reverse is observed, the GaInP was synthesized n-doped but, after the TCS preparation, the Fermi level on the TCS surface appears to be shifted to the valence band. These deviations can be explained by the presence of the surface oxidation states that lead to Fermi level pinning, which prevents assigning properly the measured BE shifts to a potential Fermi levels alignment that is expected at the junction between the bulks GaAs and GaInP.

3. Conclusion

This work serves as a proof of concept and shows that the TCS-PES is not limited to soft materials, such as perovskite solar cells, but can also be applied to hard semiconductor devices, here, III–V semiconductor stacks. Two samples, a heterointerface with distinguishable elements, Ge|GaInP, and a more complex layer stack, GaAs|GaInP, have been prepared by MOCVD. Each sample has been mechanically polished using a MULTIPREP polishing system that provides an accurate way to control the TCS angle, that is, the angle between the TCS and the bottom of the sample. The TCS preparation successfully revealed the buried Ge and GaAs substrates as well as their interface with GaInP.

Thanks to the TCS preparation, XPS line scans performed could provide chemical and electronic information about the buried interfaces. The chemical composition reveals that the GaInP layers, as well as the Ge substrate, were significantly oxidized along the TCS. The presence of surface states induces Fermi level pinning to the exposed surface of the TCS and leads to $E_F - E_{VB}$ measurements that contradict the doping levels measured by electrochemical capacitance voltage profiling of the prepared layers.

The BE shifts observed along the TCS are therefore the results of band alignments between surface states and bulk materials as well as between the two III–V semiconductors, and the two contributions, at present, cannot be discriminated. The formation of surface states during the polishing procedure prevents conclusions about the interface energetics or potential interfacial reactions that might occur during epitaxial growth of the III–V semiconductor layer structures. Therefore, additional steps for the preparation of the TCS are needed and are being investigated to limit the polishing-induced alterations. We expect that those can be reduced by preparing the TCS under controlled

© 2022 The Authors. Advanced Materials Interfaces published by Wiley-VCH GmbH

atmosphere and/or by combining the initial polishing steps with subsequent surface treatments of the exposed surfaces such as thermal annealing, or a gentle sputtering inside the cluster-tool for only removing the top oxidized surface. These treatments could possibly help to remove surface artefacts induced by the polishing process without disturbing the pristine chemical and the electronic structure of the device interface. Efforts will also be considered to have more resolved information at the interfaces. Working on more advanced PES setups (e.g., nanobeam synchrotron-based photoemission) or developing data treatment methodology considering the overlapping area are possible ways to further improve lateral resolution.

4. Experimental Section

Sample Preparation by MOCVD: All of the overlayers were grown by MOCVD in a commercial horizontal reactor (Aixtron, AIX-200) with a H_2 carrier gas on either p-Ge(100) substrate with 6° offcut toward <111> direction (Ga doped, ≈2×10^{18} cm^{-3}) or on n-GaAs(100) substrate with 0.1° offcut toward <111> direction (Si-doped, ≈2×10^{18} cm^{-3}). Tertiarybutylphosphine (TBP), trimethylindium (TMIn), trimethylgallium (TMGa) and ditertiarybutyl silane (DTBSi) were utilized as the n-dopant source, and diethylzinc (DEZn) as the p-dopant source in order to grow a 200 or 400 nm thick GaInP buffer layer. Before epitaxial growth, the GaAs(100) and Ge(100) substrates were deoxidized under tertiarybutylarsine (TBAs) at 640 °C for the first one and 650 °C for the second. The preparation of the Ge(100) substrate for the III–V epitaxy is described in more detail in a previous work.[34] Epilayers were grown at 600 °C lattice-matched to either Ge(100) or GaAs(100) substrates as confirmed ex situ by high-resolution X-ray diffractometry (HR-XRD) $\omega/2\theta$ scans (Bruker AXS D8 Discover with Ge(022)×4 asymmetric monochromator and Goebel mirror) with reference samples. The structure of the two selected samples for this study (Ge|GaInP, GaAs|GaInP) is shown in Figure S14, Supporting Information.

The carrier concentration profile in epitaxial layers was measured by electrochemical capacitance voltage profiling (ECV, WEP-CVP 21) with 0.1 M HCl solution. The p-GaInP layer on top of the Ge substrate (≈2×10^{18} cm^{-3}) had a carrier concentration of ≈2×10^{17} cm^{-3}, while for the n-GaInP layer on top of the GaAs substrate (≈2×10^{18} cm^{-3}) it equals ≈4×10^{16} cm^{-3}.

Tapered Cross Section Preparation: TCS were prepared by polishing a small angle wedge or a beveled edge with a MULTIPREP polishing system (Allied) under ambient, uncontrolled atmosphere. Samples were glued on a sample holder with a mounting wax (Allied) (see Figure S1, Supporting Information). After a proper calibration to be sure that the polishing plate was oriented parallel to the sample surface, the system allowed tuning the axial and the radial angles between the sample holder and the polishing plate with an increment of 0.02°. Sample load as well as the rotation of the plate or the duration of the polishing could also be adjusted. Diamond lapping films with a grain size of either 0.1 or 0.25 µm were used and the samples were polished dry. Detailed parameters are compiled in Table S1, Supporting Information. To date, no clear correlation between these numerous parameters and success in obtaining a favorable TCS for undistorted surface science studies has been obtained and is subject to future, systematic studies.

SEM and EDX Characterization: SEM images were obtained on a Philips XL30 FEG in secondary electron mode. Accelerating voltage, magnification, and working distance are given in the figures. EDX measurements were made in the same apparatus (SUTW, Sapphire, EDAX CDU LEAD detector). An amplification time of 100 µs had been used and an acquisition time of 60 s, leading to an energy resolution of ≈135 eV. The EDAX ZAF quantification method was used.

Photoelectron Spectroscopy Measurements: To minimize possible degradation of the samples, right after the polishing procedure they were introduced into the authors' vacuum-cluster-tool DAISY-BAT (additional information can be found here Ref. [35]). XPS was performed by using a PHI 5000 VersaProbe spectrometer and a monochromatic X-ray source (Al K_α = 1486.6 eV) set at 1.69 mA and 15 kV with a spot size of 200 µm. The lateral resolution depended not only on the X-ray spot size but also on the one of the analyzers and could be one order of magnitude lower. The XPS experiments were carried out at a base pressure below 5×10^{-9} mbar. The binding energies were calibrated with respect to the Fermi edge (E_F = 0.0 eV) of a clean Ag foil.

The high-resolution spectra were acquired with a pass energy of 23.5 eV, an electron escape angle of $\theta = 45°$, a step size of 0.2 eV and a dwell time of 100 ms, up to 20 scans were made to increase the signal-to-noise ratio. The distance between two positions on the TCS is specified in each figure. A single measurement should be enough as for device structures formed from homogeneous layers no binding energy variations perpendicular to the TCS were expected.

For the quantitative chemical analysis and the binding energy (BE) shifts, spectra were analyzed with CasaXPS (version 2.3.19PR1.0). Spectra were fitted by first, subtracting spectral background using a Shirley-type function, using weighted least-squares method and model curves (Voigt functions of 70% Gaussian and 30% Lorentzian), and *CasaXPS_kratos.lib* for the relative sensitivity factor (R.S.F.).[36]

Supporting Information

Supporting Information is available from the Wiley Online Library or from the author.

Acknowledgements

C.M. and T.M. acknowledge funding from the German Research Foundation (DFG) priority program SPP2169 (project number 423746744). M.A.Z.P., A.P., and T.H. acknowledge the CO2-WIN funding of German Federal Ministry of Education and Research BMBF through the project "DEPECOR" (BMBF) (project number 033RC021A) and by DFG through project number 424924805, HA3096/14-1 (PAK981). W.J., J.P.H., and D.C.M. acknowledge funding from DFG via project 424924805, JA859/35-1 (PAK981). The authors would also like to acknowledge K. Lakus-Wollny of TU Darmstadt for her help with the EDX mapping.

Correction added on 12 December 2022, after first online publication: Projekt Deal funding statement has been added.

Open access funding enabled and organized by Projekt DEAL.

Conflict of Interest

The authors declare no conflict of interest.

Data Availability Statement

The data that support the findings of this study are available from the corresponding author upon reasonable request.

Keywords

III-V semiconductors, buried interfaces, energetic alignment, photoelectron spectroscopy, tapered cross section

Received: July 26, 2022
Revised: October 7, 2022
Published online: December 4, 2022

© 2022 The Authors. Advanced Materials Interfaces published by Wiley-VCH GmbH

[1] F. Dimroth, M. Grave, P. Beutel, U. Fiedeler, C. Karcher, T. N. D. Tibbits, E. Oliva, G. Siefer, M. Schachtner, A. Wekkeli, A. W. Bett, R. Krause, M. Piccin, N. Blanc, C. Drazek, E. Guiot, B. Ghyselen, T. Salvetat, A. Tauzin, T. Signamarcheix, A. Dobrich, T. Hannappel, K. Schwarzburg, *Prog. Photovoltaics: Res. Appl.* **2014**, *22*, 277.
[2] J. F. Geisz, R. M. France, K. L. Schulte, M. A. Steiner, A. G. Norman, H. L. Guthrey, M. R. Young, T. Song, T. Moriarty, *Nat. Energy* **2020**, *5*, 326.
[3] M. A. Steiner, R. M. France, J. Buencuerpo, J. F. Geisz, M. P. Nielsen, A. Pusch, W. J. Olavarria, M. Young, N. J. Ekins-Daukes, *Adv. Energy Mater.* **2021**, *11*, 2002874.
[4] M. M. May, H.-J. Lewerenz, D. Lackner, F. Dimroth, T. Hannappel, *Nat. Commun.* **2015**, *6*, 8286.
[5] W. Yu, P. Buabthong, J. L. Young, Z. P. Ifkovits, S. T. Byrne, M. A. Steiner, T. G. Deutsch, N. S. Lewis, *ACS Appl. Mater. Interfaces* **2022**, *14*, 26622.
[6] M. Ben-Naim, C. W. Aldridge, M. A. Steiner, R. J. Britto, A. C. Nielander, L. A. King, T. G. Deutsch, J. L. Young, T. F. Jaramillo, *ACS Appl. Mater. Interfaces* **2022**, *14*, 20385.
[7] A. W. Bett, S. P. Philipps, S. S. Essig, S. Heckelmann, R. Kellenbenz, V. Klinger, M. Niemeyer, D. Lackner, F. Dimroth, in *28th Eur. Photovoltaic Sol. Energy Conf. Exhib.*, France (Paris) **2013**, pp. 1–6.
[8] O. Supplie, M. M. May, S. Brückner, N. Brezhneva, T. Hannappel, E. V. Skorb, *Adv. Mater. Interfaces* **2017**, *4*, 1601118.
[9] P. Schulz, D. Cahen, A. Kahn, *Chem. Rev.* **2019**, *119*, 3349.
[10] A. Klein, T. Mayer, A. Thissen, W. Jaegermann, *Methods in Physical Chemistry*, John Wiley & Sons, Ltd, New York **2012**, pp. 477–512.
[11] L. Meier, C. Braun, T. Hannappel, W. G. Schmidt, *Phys. Status Solidi B* **2021**, *258*, 2000463.
[12] L. Meier, W. G. Schmidt, *Phys. Status Solidi B* **2022**, *259*, 2100462.
[13] A. Beyer, K. Volz, *Adv. Mater. Interfaces* **2019**, *6*, 1801951.
[14] L. Ostheim, P. J. Klar, Y. Moryson, M. Rohnke, A. Beyer, M. Volk, M. Munde, W. Stolz, K. Volz, *J. Appl. Phys.* **2019**, *126*, 215704.
[15] A. Beyer, M. S. Munde, S. Firoozabadi, D. Heimes, T. Grieb, A. Rosenauer, K. Müller-Caspary, K. Volz, *Nano Lett.* **2021**, *21*, 2018.
[16] Y. Dong, R. M. Feenstra, M. P. Semtsiv, W. T. Masselink, *J. Appl. Phys.* **2008**, *103*, 073704.
[17] H. Han, A. Beyer, J. Belz, A. König, W. Stolz, K. Volz, *J. Appl. Phys.* **2017**, *121*, 025301.
[18] S. Dhellemmes, S. Godey, A. Wilk, X. Wallart, F. Mollot, *J. Cryst. Growth* **2005**, *278*, 564.
[19] M. C. López-Escalante, M. Gabás, I. García, E. Barrigón, I. Rey-Stolle, C. Algora, S. Palanco, J. R. Ramos-Barrado, *Appl. Surf. Sci.* **2016**, *360*, 477.
[20] O. Romanyuk, A. Paszuk, I. Gordeev, R. G. Wilks, S. Ueda, C. Hartmann, R. Félix, M. Bär, C. Schlueter, A. Gloskovskii, I. Bartoš, M. Nandy, J. Houdková, P. Jiříček, W. Jaegermann, J. P. Hofmann, T. Hannappel, *Appl. Surf. Sci.* **2022**, *605*, 154630.
[21] A. Klein, W. Jaegermann, *ECS J. Solid State Sci. Technol.* **2020**, *9*, 093012.
[22] O. Romanyuk, I. Gordeev, A. Paszuk, O. Supplie, J. P. Stoeckmann, J. Houdkova, E. Ukraintsev, I. Bartoš, P. Jiříček, T. Hannappel, *Appl. Surf. Sci.* **2020**, *514*, 145903.
[23] M. Wussler, T. Mayer, C. Das, E. Mankel, T. Hellmann, C. Prawobo, I. Zimmermann, M. K. Nazeeruddin, W. Jaegermann, *Adv. Funct. Mater.* **2020**, *30*, 1910679.
[24] C. Das, M. Wussler, T. Hellmann, T. Mayer, I. Zimmermann, C. Maheu, M. K. Nazeeruddin, W. Jaegermann, *ACS Appl. Mater. Interfaces* **2020**, *12*, 40949.
[25] C. Das, W. Zia, C. Mortan, N. Hussain, M. Saliba, J. I. Flege, M. Kot, *Sol. RRL* **2021**, *5*, 2100298.
[26] M. P. Seah, W. A. Dench, *Surf. Interface Anal.* **1979**, *1*, 2.
[27] A. Ohta, H. Nakagawa, H. Murakami, S. Higashi, S. Miyazaki, *e-J. Surf. Sci. Nanotechnol.* **2006**, *4*, 174.
[28] I. Z. Mitrovic, M. Althobaiti, A. D. Weerakkody, V. R. Dhanak, W. M. Linhart, T. D. Veal, N. Sedghi, S. Hall, P. R. Chalker, D. Tsoutsou, A. Dimoulas, *J. Appl. Phys.* **2014**, *115*, 114102.
[29] G. Chen, S. B. Visbeck, D. C. Law, R. F. Hicks, *J. Appl. Phys.* **2002**, *91*, 9362.
[30] S. C. Ghosh, M. C. Biesinger, R. R. LaPierre, P. Kruse, *J. Appl. Phys.* **2007**, *101*, 114321.
[31] K. Ibrahim, F. Q. Liu, J. F. Jia, Y. H. Dong, Y. Yang, H. J. Qian, S. H. Lu, S. C. Wu, Z. N. Gu, *J. Electron Spectrosc. Relat. Phenom.* **1996**, *78*, 437.
[32] A. J. Murrell, A. T. S. Wee, D. H. Fairbrother, N. K. Singh, J. S. Foord, G. J. Davies, D. A. Andrews, *J. Appl. Phys.* **1990**, *68*, 4053.
[33] H. A. Budz, M. C. Biesinger, R. R. LaPierre, *J. Vac. Sci. Technol., B: Microelectron. Nanometer Struct.–Process., Meas., Phenom.* **2009**, *27*, 637.
[34] A. Paszuk, O. Supplie, S. Brückner, E. Barrigón, M. M. May, M. Nandy, A. Gieß, A. Dobrich, P. Kleinschmidt, I. Rey-Stolle, T. Hannappel, *Appl. Surf. Sci.* **2021**, *565*, 150513.
[35] G. Cherkashinin, J. Schuch, B. Kaiser, L. Alff, W. Jaegermann, *J. Phys. Chem. Lett.* **2020**, *11*, 3754.
[36] N. Fairley, V. Fernandez, M. Richard-Plouet, C. Guillot-Deudon, J. Walton, E. Smith, D. Flahaut, M. Greiner, M. Biesinger, S. Tougaard, D. Morgan, J. Baltrusaitis, *Appl. Surf. Sci. Adv.* **2021**, *5*, 100112.

© 2022 The Authors. Advanced Materials Interfaces published by Wiley-VCH GmbH